NASA-CR-203112

RESEARCH IN NONLINEAR FLIGHT CONTROL FOR TILTROTOR AIRCRAFT OPERATING IN THE TERMINAL AREA.

Progress Report #1
November 1996

1 September 1995 - 31 August 1996

Research supported by the NASA Ames Research Center
NASA Cooperative Agreement No. NCC 2-922

Principal Investigator: Dr. A. J. Calise
Research Assistant: R. Rysdyk
NASA Grant Monitor: Dr. R. Chen

School of Aerospace Engineering
Georgia Institute of Technology
Atlanta, Georgia 30332

Contents

List of Tables

List of Figures

Summary

The research during the first year of the effort focused on the implementation of the recently developed combination of neural net work adaptive control and feedback linearization. At the core of this research is the comprehensive simulation code *Generic Tiltrotor Simulator* (GTRS) of the XV-15 tiltrotor aircraft. For this research the GTRS code has been ported to a Fortran environment for use on PC.

The emphasis of the research is on terminal area approach procedures, including conversion from aircraft to helicopter configuration. This report focuses on the longitudinal control which is the more challenging case for augmentation. Therefore, an *attitude command attitude hold* (ACAH) control augmentation is considered which is typically used for the pitch channel during approach procedures.

To evaluate the performance of the neural network adaptive control architecture it was necessary to develop a set of low order pilot models capable of performing such tasks as,

- follow desired altitude profiles,
- follow desired speed profiles,
- operate on both sides of powercurve,
- convert, including flaps as well as mastangle changes,
- operate with different *stability and control augmentation system* (SCAS) modes.

The pilot models are divided in two sets, one for the backside of the powercurve and one for the frontside. These two sets are linearly blended with speed. The mastangle is also scheduled with speed.

Different aspects of the proposed architecture for the neural network (NNW) augmented model inversion were also demonstrated. The demonstration involved implementation of a NNW architecture using linearized models from GTRS, including rotor states, to represent the XV-15 at various operating points. The dynamics used for the model inversion were based on the XV-15 operating at 30 Kts, with residualized rotor dynamics, and not including cross coupling between translational and rotational states. The neural network demonstrated ACAH control under various circumstances.

Future efforts will include the implementation into the Fortran environment of GTRS, including pilotmodeling and NNW augmentation for the lateral channels. These efforts should lead to the development of architectures that will provide for fully automated approach, using similar strategies.

1 Background

The objective of the current research effort is to develop nonlinear flight control algorithmes for tiltrotor aircraft operating in the airport terminal area. Like no other aircraft, the tiltrotor displays varying stability and control characteristics. Most conventional flight control architectures provide for mission specific augmentation but are not flexible enough to ensure significant improvements over the entire range of operating circumstances. In the case of tiltrotor aircraft, examples include the transition from fixed wing to rotary wing flight, mixing of controls, and the possible failure of actuators and its consequences. In the course of this research several levels of the flight control will be investigated. These include inner loop SCAS at the lowest level, automated degrees of freedom at the medium level, and at the highest level fully automated trajectory following control in the airport terminal area. The study encompasses all flight modes including helicopter mode, transition and airplane mode. A key aspect of this study is the accomodation of modeling error and failure modes. Therefore, recent developments in combining NNWs and feedback linearization will be exploited. The research builds upon the NNW flight control studies that have been done at Georgia Tech to date. These studies addressed;

- Full envelope flight control design without the need for gain scheduling,
- real time adaption to uncertain nonlinear effects, and
- the ability to adapt to partial failures in actuators.

The use of adaptive NNWs in these studies represent a unique application in the aerospace field in the sense that they are online, adapting while controlling, with guaranteed stability properties. The stability properties derive from Lyapunov theory used in the design of the learning rules for the adaptation of the NNW. Similar control strategies where successfully applied to comprehensive simulations of an F/A-18 airplane [1] and an AH-64 helicopter [2]. A SCAS system for a tiltrotor aircraft with its ability to convert from airplane to helicopter configuration, is the ideal candidate to benefit from a control architecture as presented in the current research effort.

2 Flight Control Augmentation

In this report two types of control augmentation are mentioned, *Rate Command Attitude Hold* and *Attitude Command Attitude Hold.* These specifications each cover two aspects of the response to a particular input, the *Command* and the *Hold* or *Stabilization* part. Table 1 shows various types of augmentation for different channels, ordered from least to most stabilization. Reference [3] gives the full time automatic flight control system features for the V-22 tiltrotor aircraft. This is summarized in table 2.

Table 1: Combinations of control augmentation response types, from least to most stabilization, from [4].

	Response Type:	Used for:
1	Rate	Vertical T/O and transition clear of earth
2	ACAH+RCHH	Slope Landing, precision vertical landing
3	ACAH+RCHH+RCAltH	Precision hover and vertical T/O and transition
4	Rate+RCHH+RCAltH+PosH	Tasks involving 'divided attention'
5	ACAH+RCHH+RCAltH+PosH	Rapid hovering turn
6	TRC+RCHH+RCAltH+PosH	Hover and taxi, vertical T/O and transition

where,

Rate	=	Rate or Rate Command Attitude Hold (RCAH)
TC	=	Turn Coordination
ACAH	=	Attitude Command Attitude Hold
RCAltH	=	Rate Command Altitude Hold
HH	=	Heading Hold
RCHH	=	Rate Command Heading Hold
PosH	=	Position Hold response type
TRC	=	Translational Rate Command

Table 2: V-22 tilt rotor control augmentation response types.

	Hover		Fwd Flight	
Axis	Command	Hold	Command	Hold
Pitch	Att	Att	'Att'	Att
Roll	Rate	Att	Rate	Att
Wing Lvlr	Att	Att	Att	Att
Yaw	Rate	HH	Lat Acc	HH/TC
HH Off	Rate	Rate	Lat Acc	TC
Thrust/Pwr	Thrust	Vert. Rate	Thrust	

2.1 Rate Command and Attitude Command

Reference [4] defines the *Command* part of the augmentation by considering a control step input. A control system with a SCAS setting referred to as *Attitude-Command* implies that the aircraft responds with a proportional attitude given a step control input. Similarly, a control system with a SCAS setting referred to as *Rate-Command* implies that the aircraft responds with a proportional attitude rate of change given a step control input.

2.2 Attitude Hold

Attitude Hold, also referred to as *Attitude Stabilization*, is defined using a pulse input into the primary control, see figure 1. It implies that the aircraft attitude will be returned to its original value, given no other inputs.

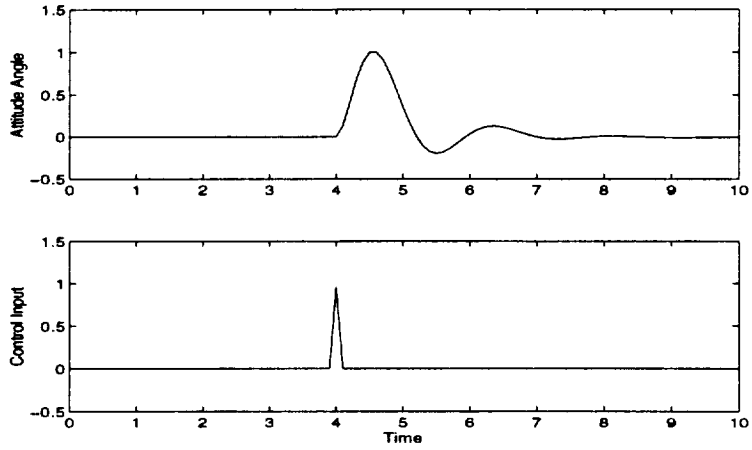

Figure 1: Control with attitude hold augmentation.

2.3 Augmentation for an Instrument Approach

Reference [5] describes two experiments with a 40,000 lbf civil tiltrotor piloted simulation on steep instrument approaches. The control system is indicated as an ACAH for pitch and roll, and the yaw axis augmentation included *Heading Hold* at speeds smaller than 40 Kts and *Turn Coordination* at speeds bigger than 80 Kts with linear blending between them. This article represents an example for typical approach procedures that a pilot might follow in performing terminal area operations with a civilian tiltrotor aircraft. The considerations involved in such a procedure include;

- a schedule for conversion of mast angle with speed, from airplane to helicopter in the regular approach and vice versa for a missed approach procedure,

- deployment or retraction of flaps depending on mastangle, speed, and glide slope,
- switching from RCAH to ACAH augmentation mode,
- desired altitude and speed trajectories.

Reference [5] and the considerations listed here were used to develop the set of pilot models described in section 3.

3 Low Order Pilot Models for Longitudinal Operation of a Tiltrotor Aircraft

To evaluate the performance of a neural network adaptive control architecture it will be necessary to provide for a pilot model. This pilot model should be able to operate the tiltrotor smoothly in various parts of the operating envelope. Therefore, the objective is to create such a model that can be tailored to specific tasks, and configured to respond slow enough to maintain a distinction between inner loop network adaptive control and pilot activity. The model is to perform such tasks as,

- follow desired altitude profiles,
- follow desired speed profiles,
- operate on both sides of powercurve,
- convert, including flaps as well as mastangle changes,
- operate with different SCAS modes.

This section describes a combination of low order pilot models for the longitudinal channels only. The pilot model consists of two parts, one *backside pilot* (BSP) and one *frontside pilot* (FSP). These two parts are linearly blended with speed. The results using this pilot show:

- Conversion both ways can be achieved with reasonable tracking.
- Fairly aggressive accelerations and climb rates can be achieved.
- The pilot model can be adjusted for different operating circumstances.
- The pilot model can be modified to reflect more accurately the physiological and psychological behaviour of a human being. However, the emphasis in this work is on operation of the vehicle.

The airplane considered will be operated with stabilizing SCAS systems. Furthermore, the maneuvers considered here are not aggressive and do not need modeling of the fast characteristics of neurological and muscular time constants. The longitudinal pilot models were adjusted for operation under an ACAH SCAS, described in section 2. This mode does not work well at higher speeds when trying to maintain a desired altitude and speed. A setup that allows for switching

between modes at certain operating points needs to be added. A similar lateral pilot also needs to be created. However, the longitudinal modeling problem is far more challenging than the lateral problem.

3.1 Tiltrotor Aircraft Low Order Response Approximations

The true aircraft is represented by the Generic Tiltrotor Simulation program that was jointly developed by NASA and Boeing. The model represents the XV15 tiltrotor aircraft. This aircraft can operate both as a conventional helicopter, and as a regular airplane for the higher speeds. In this modeling work the pure helicopter mode is used under 60 Kts and the pure airplane mode is used above 120 Kts. The possibility to convert between the two modes requires operation on both sides of the powercurve. From a modelling perspective that means a total change in the function of the controls and the associated responses of the aircraft. This section describes the aircraft responses to inputs in the longitudinal control channels in the two different configurations.

Powercurve

The *powercurve* refers to the graph of power required versus flight speed. The typical curve for a helicopter shows a need for high power at hover, due to the powered lift condition. As shown in figure 2, the need for power decreases as the speed increases. This trend continues until the aerodynamic drag becomes the dominant factor at higher speeds. The lowest point of the powercurve for a tiltrotor occurs between the helicopter and airplane configuration. The significance of the powercurve is in the fact that it demands a different control strategy at the different operating points along the curve. The change in control strategy is centered around the lowest point of the powercurve. For the conversion schedule used in this work this point occurs between 70 and $100 Kts$. Not all the subtleties associated with the powercurve are considered here. However, it did lead to the idea of the pilot blending. The blending architecture is described in section 3.2.

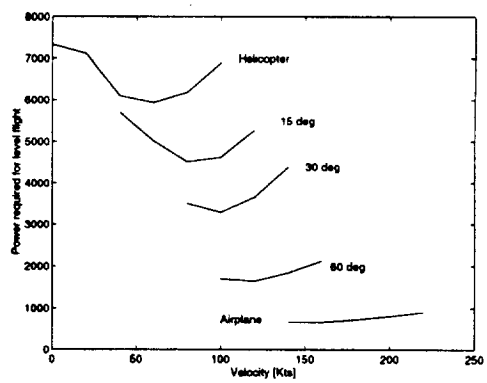

Figure 2: Powercurve for different configurations.

Longitudinal Stick Command Response, Helicopter Configuration

In helicopter configuration the speed is controlled by a deflection of the longitudinal stick. A positive deflection is forward, which results in a positive acceleration of the helicopter. As the speeds increases, so does the aerodynamic drag, therefore a step response in the longitudinal stick results in the acceleration profile illustrated in figure 3. A low order model of this behaviour is given by,

$$\frac{\dot{U}}{\delta_{xln}} = \frac{K_{ac}s}{s^2 + a_1 s + a_0} \tag{1}$$

or equivalently,

$$\frac{U}{\delta_{xln}} = \frac{K_{ac}}{s^2 + a_1 s + a_0} \tag{2}$$

with parameters,

$$\begin{aligned} K_{ac} &= 3.0 \\ a_1 &= 1.02 \\ a_0 &= .06 \end{aligned}$$

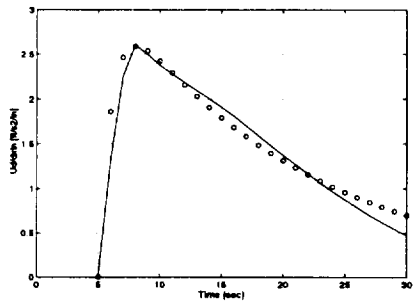

Figure 3: Udot/dxln step response at 30 Kts.

Power Lever Command Response, Helicopter Configuration

The response to a step input to the collective lever is illustrated in figure 4. This suggests that the response is first order, and can be accurately modeled using,

$$\frac{\dot{h}}{\delta_{xcol}} = \frac{K_{ac}}{s + c} \tag{3}$$

Some relevant parameter values at different airspeeds are given in the table 3. The pilot model development in the next section was based on the values at 30 Kts.

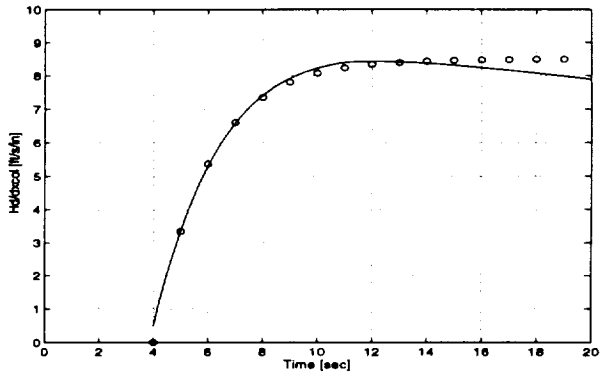

Figure 4: Hdot/dxcol step response at 30Kts.

Table 3: Vertical rate response model parameter values at 30 Kts.

V $[Kts]$	K $[(ft/s)/in/s]$	c $[s^{-1}]$
0	2.26	.19
30	4.25	.50
70	4.75	.625

Longitudinal Stick Command Response in Airplane Configuration

In airplane configuration the longitudinal stick is used for altitude control. The primary effect of a longitudinal input is a pitch change. Thus the pilot is controlling altitude as a secondary effect. Another secondary effect due to longitudinal stick input is a change in velocity. The step response to longitudinal stick input in forward flight is illustrated in figure 5. The second order model is given by,

$$\frac{\dot{H}}{\delta_{xln}} = \frac{-K_{ac} \cdot s}{s^2 + a_1 s + a_0} \tag{4}$$

In terms of altitude control this is equivalent to,

$$\frac{H}{\delta_{xln}} = \frac{-K_{ac}}{s^2 + a_1 s + a_0} \tag{5}$$

The parameters were found to be,

$$\begin{aligned} a_1 &= .54 \\ a_0 &= .0329 \\ K_{ac} &= -15.28 \end{aligned}$$

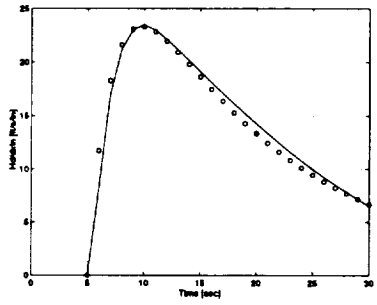

Figure 5: Hdot/dxln step response at 180 Kts.

Power Lever Command Response, Airplane Configuration

In forward flight the altitude and speed are both secondary effects of the pitch control. To reduce this coupling effect, feedback of *energy per unit weight* was used to define the throttle pilot. From the response characteristics at 180 Kts illustrated in figure 6, a low order model of the airplane response is given by,

$$\frac{\dot{E}}{\delta_{xcol}} = \frac{K_{ac}}{(\tau \cdot s + 1)} \tag{6}$$

with,

$$\begin{aligned} K_{ac} &= 160 \\ \tau_{ac} &= .2 \end{aligned}$$

Here E is the energy per unit mass,

$$E = H + \frac{V^2}{(2 \cdot g)} \tag{7}$$

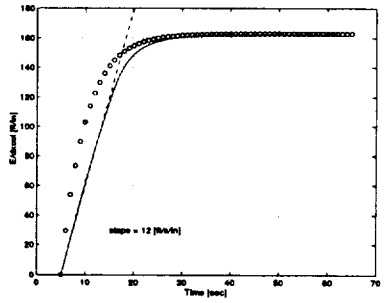

Figure 6: E/dxcol step response at 180 Kts.

3.2 Pilot Model Design

The pilot model was developed on the basis of the following form for the pilot transfer function

$$G_{plt} = \frac{K_{plt}(s+\beta)}{(s+\alpha)} \tag{8}$$

This form permits the pilot to be represented as either a lead compensator, a lag compensator, or a P+I controller. As illustrated in figures 7 and 8, the pilot models will be implemented in a closed loop with the aircraft. The same transfer function form is used to model pilot response to airplane response in the form of the stick and power lever input.

The pilot models for the helicopter configuration are combined with those for the airplane configuration through convex blending. The convex blending is linear, as indicated in figure 9, and implemented as follows

$$\delta_x = (1-\alpha)\cdot\delta_{Heli} + \alpha\cdot\delta_{Airpln} \tag{9}$$

where,

$$\begin{array}{lcccccc} \alpha & = & 1 & if & & V & > & VII \\ \alpha & = & \frac{V-VI}{VII-VI} & if & VI \leq & V & \leq & VII \\ \alpha & = & 0 & if & & V & < & VI \end{array}$$

with V representing the aircraft speed, and the authority for the helicopter and airplane pilots represented respectively by the weights, $(1-\alpha)$ and α. The low speed pilot models have full authority at 30 Kts and below. The the high speed models have full authority at 140 Kts and above. This choice of VI and VII reflects the fact that the lowest point in the powercurve occurs between 70 and 100 Kts, depending on the conversion schedule, and flight configuration.

Root locus methods were used to select desirable closed loop characteristics. The pilot models are represented here in continuous time. The actual implementation in the Generic Tiltrotor Simulation is a $.01sec$ zero order hold discrete time representation.

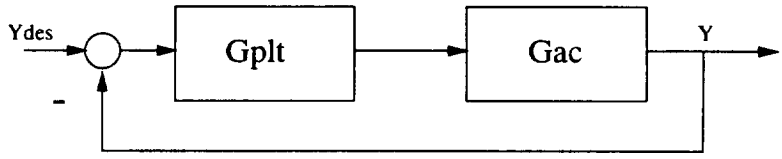

Figure 7: Closed loop of pilot model with aircraft.

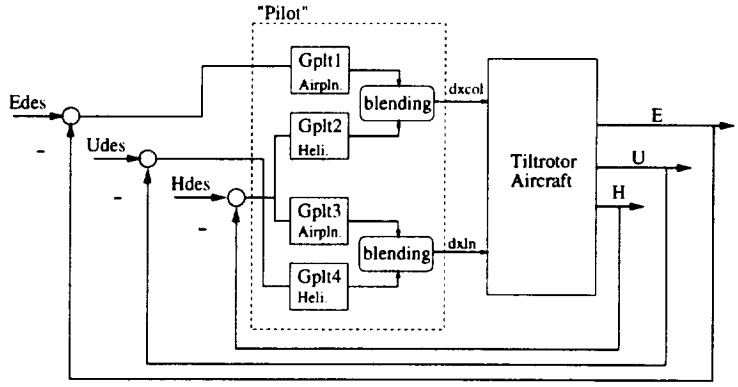

Figure 8: Implementation of pilot models.

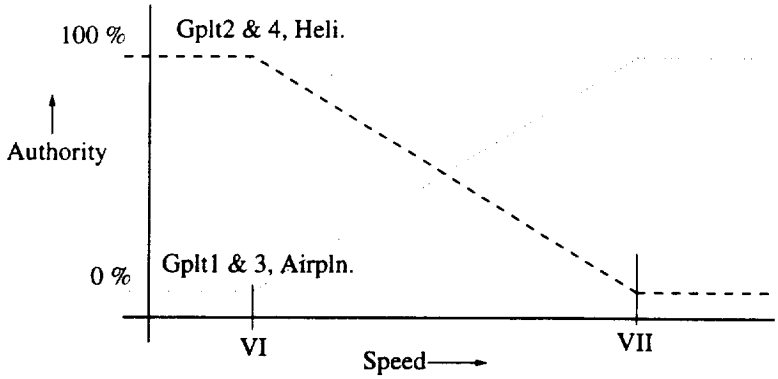

Figure 9: Blending of pilot models.

Pilot for Speed Control in Helicopter Configuration

The speed at hover is controlled by the longitudinal stick input. The tiltrotor in helicopter configuration at 30 Kts was found to behave as follows,

$$\frac{U}{\delta_{xln}} = \frac{K_{ac}}{s^2 + a_1 s + a_0} \tag{10}$$

where,

$$\begin{aligned} K_{ac} &= 3.0 \\ a_1 &= 1.02 \\ a_0 &= .06 \end{aligned}$$

The design of the pilot is based on the pilot acting as a P+I controller. A blockdiagram representing the closed loop is shown in figure 10. Figure 11 shows root loci plots for two values of β. Selecting $\zeta = .9$ and $\omega_n = .33$ for the dominant closed loop poles results in

$$\begin{aligned} K_{plt} &= .10 \\ \beta &= .15 \end{aligned}$$

and,

$$G_{plt} = \frac{.1 \cdot (s + .15)}{s}$$

The performance is shown as a response to a step in Udes in figures 12 and 13.

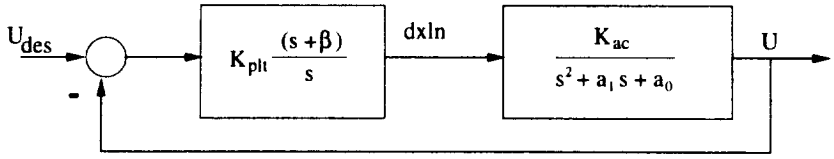

Figure 10: Pilot model for speed in helicopter configuration.

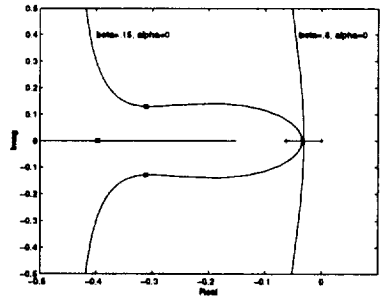

Figure 11: Root locus for helicopter speed control.

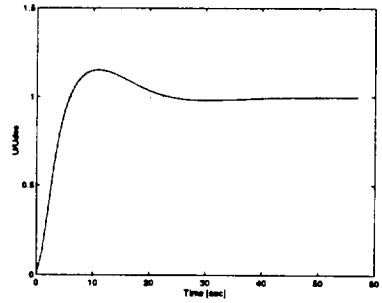

Figure 12: Pilot performance for 10 Kts step in Udes in helicopter configuration.

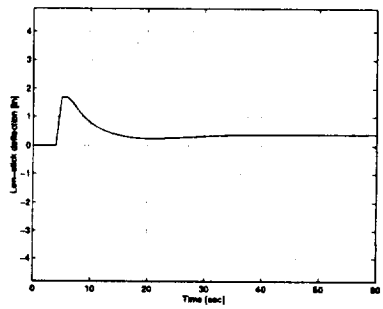

Figure 13: Pilot control activity for a 10 Kts step in Udes in helicopter configuration.

Pilot for Altitude Control in Helicopter Configuration

The pilot model for the collective control was optimized for operation point at 30 Kts, at 13,000 lbf and a flap/flaperon setting of 40°/25°. Test inputs into the collective lever of the aircraft showed its vertical rate response to be,

$$\frac{\dot{h}}{\delta_{zcol}} = \frac{4.25}{s + .5}$$

The blockdiagram of the altitude pilot is shown in figure 14. This is a type 1 system. The closed loop transfer function is given by

$$\frac{H}{H_{des}} = \frac{\tilde{K}(s + \beta)}{s^3 + s^2(\alpha + c) + s(\alpha \cdot c + \tilde{K}) + \tilde{K}\beta} \tag{11}$$

where $\tilde{K} = K_{ac} \cdot K_{plt} = 4.25 \cdot K_{plt}$, and $c = .5$. The steady state error is zero if the first order model for the vertical rate is a reasonable representation. The design for this model resulted in

$$\begin{aligned} K_{plt} &= .75 \\ \alpha &= 2.9 \\ \beta &= .8 \end{aligned}$$

Once a selection of α and β is made, the gain can be adjusted for mild or more aggressive pilot behaviour. From a root locus analysis of $G_{plt}G_{ac}$ it is possible to select, for example, a $T_{setl} \approx 10sec$, $\zeta = 1$ or a $T_{setl} \approx 3sec$, $\zeta = .7$. The root locus of $G_{plt}G_{ac}$ for these examples is given in figures 15 and 16. A milder setting for the model is then,

$$\begin{aligned} K_{plt} &= .075 \\ \alpha &= 2.9 \\ \beta &= .8 \end{aligned}$$

with a $\zeta = 1$ and $\omega_n = .3$. The pilot performance is displayed in figures 17 and 18.

In a large altitude or flight level change, a human pilot will use the vertical speed indicator to monitor the rate of descend. The closed loop transfer function of the vertical rate control loop at hover, from figure 19, is

$$\frac{\dot{H}}{\dot{H}_{des}} = \frac{\tilde{K}(s + \beta)}{s + (\alpha + c + \tilde{K})s + (\alpha \cdot c + \beta\tilde{K})} \tag{12}$$

Here the desired response can be determined by selecting,

$$\begin{aligned} (\alpha + c + K_{ac}K_p) &= 2\zeta\omega_n \\ (\alpha \cdot c + K_{ac}K_p\beta) &= \omega_n^2 \end{aligned}$$

Selecting $\alpha = 0$ to obtain zero steady state error, with $c = .5$ and $K_{ac} = 4.25$ the current design is based on $\zeta = .9$ and $\omega_n = 1.5$, thus giving $K_{plt} = .35$, and $\beta = .8$. The resulting performance to a $1000fpm$ step in R.O.C. is shown in figure 20. The response to a requested change in flight level would require the pilot to initially establish a desired vertical rate, then once the desired new

altitude is almost established the pilot will concentrate on the altimeter again. This strategy is reflected in a convex blending of the altitude and rate models described above, as indicated in figure 21. The convex blending is linear and implemented as follows,

$$\delta_{xcol} = (1 - \eta) \cdot \delta_{xcolH} + \eta \cdot \delta_{xcol\dot{H}} \tag{13}$$

where,

$$\begin{array}{rcccccl} \eta & = & 1 & if & & \tilde{H} & > 50 \\ \eta & = & \frac{\tilde{H}-25}{50-25} & if & 25 \leq & \tilde{H} & \leq 50 \\ \eta & = & 0 & if & & \tilde{H} & < 25 \end{array}$$

with $\tilde{H} = H_{des} - H$ the altitude error signal. A combination of this rate and altitude response is shown in figures 22 and 23.

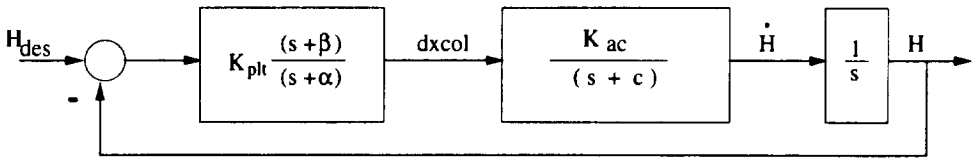

Figure 14: Pilot model for altitude in helicopter configuration.

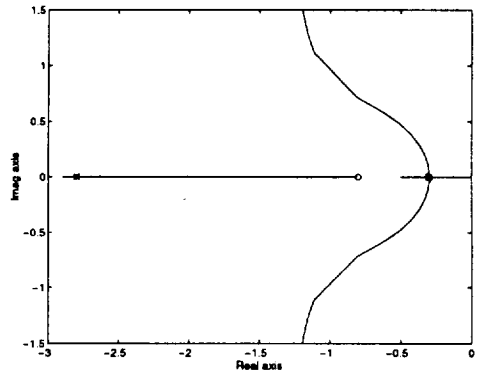

Figure 15: Altitude loop root locus, mild ($T_{setl} = 10sec$) pole locations.

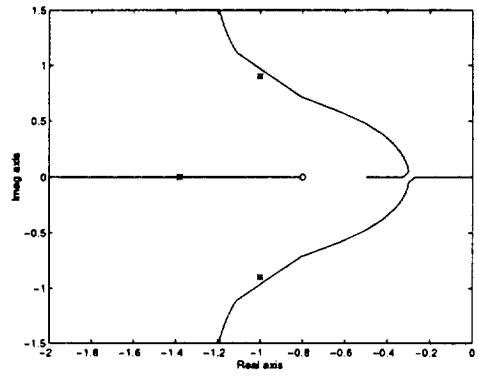

Figure 16: Altitude loop root locus, aggressive ($T_{setl} = 3sec$) pole locations.

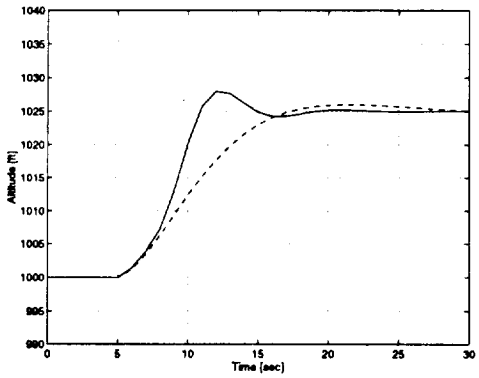

Figure 17: Pilot performance for 25 ft step in Hdes in helicopter configuration with mild and aggressive pilot model design.

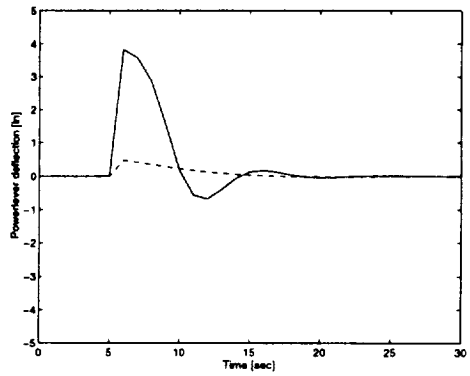

Figure 18: Collective control activity for 25 ft step in Hdes in helicopter configuration with mild and aggressive pilot model design.

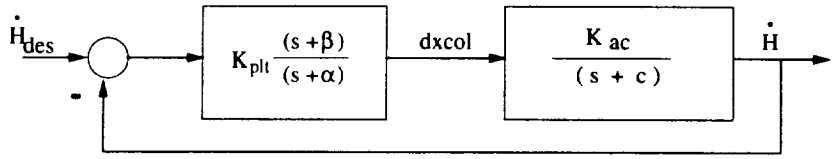

Figure 19: Vertical rate in helicopter configuration.

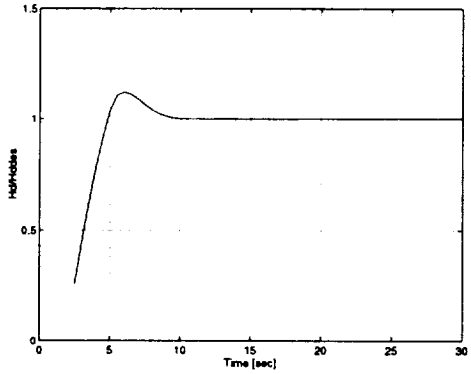

Figure 20: Pilot performance for 16.7 ft/s step in R.O.C. in helicopter configuration.

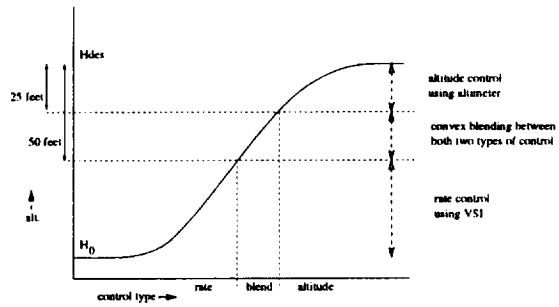

Figure 21: Vertical rate to altitude control transition.

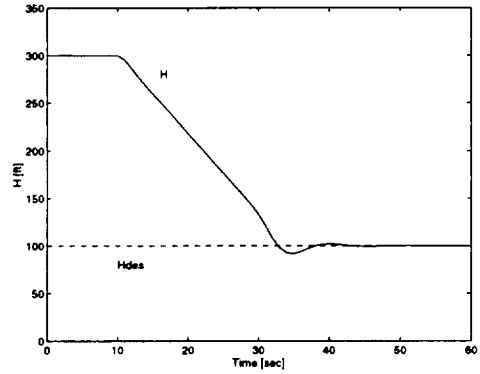

Figure 22: Pilot performance -200 ft step in altitude in helicopter configuration.

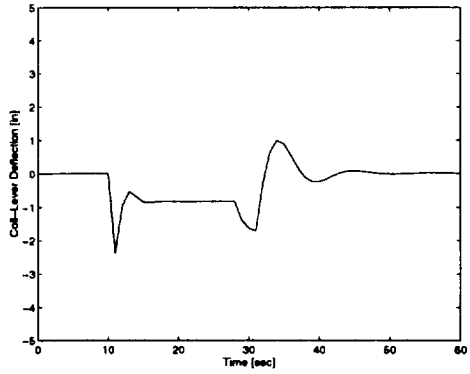

Figure 23: Pilot control activity for -200 ft step in altitude in helicopter configuration.

Pilot for Altitude Control in Airplane Configuration

The longitudinal channel at forward flight showed a second order response as follows,

$$G_{ac} = \frac{\dot{H}}{\delta_{xln}} = \frac{-K_{ac} \cdot s}{s^2 + a_1 s + a_0} \tag{14}$$

The parameters were found to be,

$$\begin{aligned} a_1 &= .54 \\ a_0 &= .0329 \\ K_{ac} &= -15.28 \end{aligned}$$

Selecting $T_{setl} = 6\ sec$, and $\zeta = .707$ as desirable for the dominate closed loop poles results in

$$\begin{aligned} K_{plt} &= -.003 \\ \alpha &= .63 \\ \beta &= .46 \end{aligned}$$

With this selection the steady state error for a step input is 36%. However, since the altitude pilot model is blended with a vertical rate pilot model, the altitude steps are limited to 50 ft or less (see below), which will result in an $18ft$ deviation. A zero steady state error can be achieved by setting $\alpha = 0$. A $T_{setl} \approx 12sec$ with low damping, $\zeta = .5$, is then possible. The results are,

$$\begin{aligned} K_{plt} &= -.016 \\ \beta &= .04 \end{aligned}$$

The vertical rate control loop in airplane configuration is shown in figure 24. Modeling the pilot as a P+I controller (α=0), the closed loop transfer function is given by

$$\frac{\dot{H}}{\dot{H}_{des}} = \frac{\tilde{K}(s + .8)}{s^2 + (a_1 + \tilde{K})s + (a_0 + .8\tilde{K})} \tag{15}$$

Here the desired response can be selected by ζ, and ω_n, then β and K_{plt} are determined from,

$$\begin{aligned} (a_1 + K_{ac}K_p) &= 2\zeta\omega_n \\ (a_0 + K_{ac}K_p \cdot \beta) &= \omega_n^2 \end{aligned}$$

Based on a $\zeta = 1$ and $T_{setl} \approx 6\ sec$ the pilot model is given by $K_{plt} = -.03$ and $\beta = .47$. The resulting performance is displayed in figure 25.

As is the case in altitude control in the helicopter configuration, the response to a requested change in flight level is based on a combination of altitude and rate tracking. This control strategy for δ_{lon} is similar to that described for δ_{col} in equation 13. Figure 26 shows the response of the aircraft with altitude and vertical rate pilot combined. Figure 27, shows the rate of climb response to achieve the $1000ft$ altitude change. Figure 28 displays the corresponding pilot activity.

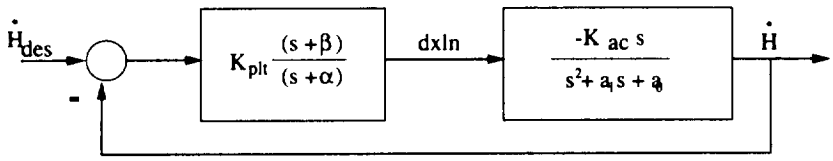

Figure 24: Pilot model for vertical rate in airplane configuration.

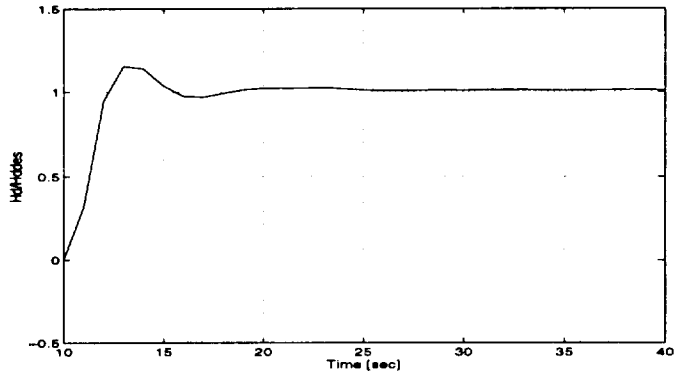

Figure 25: Hd/Hddes in response to 1000fpm step.

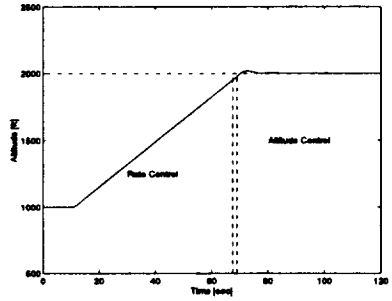

Figure 26: Altitude profile in response to Hdes +1000 ft at 180 Kts.

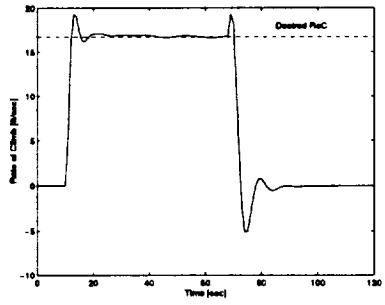

Figure 27: Rate of climb in response to Hdes +1000ft at 180 Kts.

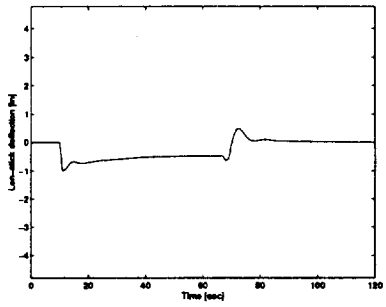

Figure 28: Pilot control activity in response to Hdes +1000ft at 180 Kts.

Pilot for Speed Control in Airplane Configuration

At hover the primary control for altitude is the collective lever. In forward flight there is no primary control for altitude. Instead, the pilot changes altitude by controlling pitch. A change in pitch will result in secondary responses that affect the altitude and speed. The collective lever has a primary response that affects both altitude and speed, depending on the mast angle of the rotor/propellors. It is therefore convenient to consider the collective lever to be the primary control for energy rather than speed. The energy per unit weight can be written as,

$$E = H + \frac{V^2}{2g} \tag{16}$$

Using the throttle to close the loop over the energy, the pilot can be implemented according to figure 29. From the response characteristics at 180 Kts the low order model of the airplane is presented as,

$$\frac{\dot{E}}{\delta_{xcol}} = \frac{160}{(0.2s+1)}$$

The transfer function from desired energy to actual energy according to this model is then,

$$\frac{E}{E_{des}} = \frac{5\tilde{K}(s+\beta)}{s^3 + s^2 \cdot 5(1+.2\alpha) + s \cdot 5(\alpha+\tilde{K}) + 5\tilde{K}\beta} \tag{17}$$

With the selection of $\alpha = .05$ to provide the smallest possible ramp tracking error, and selecting $\zeta = 1$ and $\omega_n = .3$ results in,

$$\begin{aligned} K_{plt} &= .003 \\ \beta &= .16 \end{aligned}$$

The resulting performance to a step in udes is shown in figures 30 and 31. The high frequency content visible in figure 30 is caused by the ACAH SCAS mode combined with the high pitch angles involved in this maneuvre. This can be improved by letting the pilot model switch the airplane to RCAH once a forward flight configuration is established. Since the emphasis of this work is on terminal approach operations, in which ACAH SCAS is normally selected, no pilot models for RCAH augmentation were developed in this initial effort.

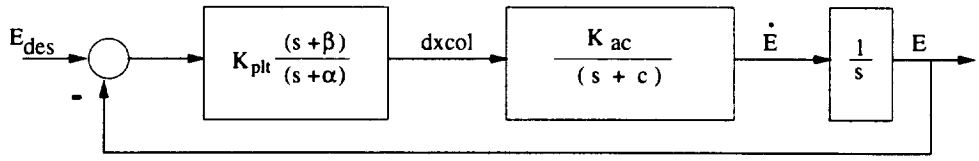

Figure 29: Pilot model for control of energy in airplane configuration.

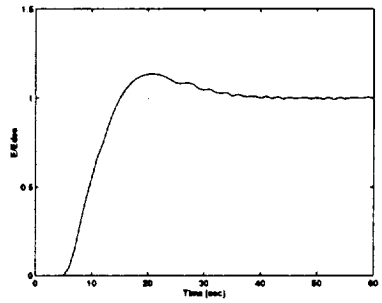

Figure 30: Pilot performance for step in Udes in airplane configuration.

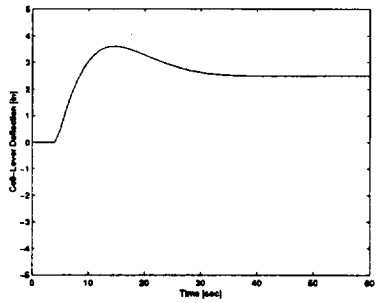

Figure 31: Pilot control activity for step in Udes in airplane configuration.

3.3 Pilot Performance in Different Phases of Flight

Conversion

In reference [5] a conversion schedule representative for a civilian tiltrotor is indicated to be a deceleration of $-.01G$ *force*, performed at constant altitude. This conversion was simulated with the pilot model developed in the preceding section. The pilot model can also be tuned to perform conversions with decelerations up to $-.1G$ *force*. This will allow for a conversion in less than a minute as shown in figures 32 and 33. Though not representative for manoeuvres of a civilian tiltrotor, it is included here as an indication of model performance. The performance in transition flight with the more representative deceleration of $-.01G$ *force* is shown in figures 34 and 35. These figures show a 2 minute time history, starting with the airplane in trimmed flight at 110 Kts and with a mastangle of 60 degrees from vertical, and ending in a configuration with a mastangle of 15 degrees at 70 Kts.

The last stage of an instrument approach to an airport will require a descent to *Minimum Descent Altitude*, MDA. Ideally, this would be a steep approach for noise abatement. To verify pilot performance for this stage of flight a 500 foot descend was commanded at $30Kts$ in helicopter configuration with a $1000fpm$ descend rate. This is equivalent to a glide slope of approximately $18°$. The results are shown in figures 36 and 37. The minimum descent altitude is violated by $10ft$. The $1000fpm$ can be considered fairly aggressive, and serves only as an illustration. A true descend would probably involve a $500fpm$ sink rate.

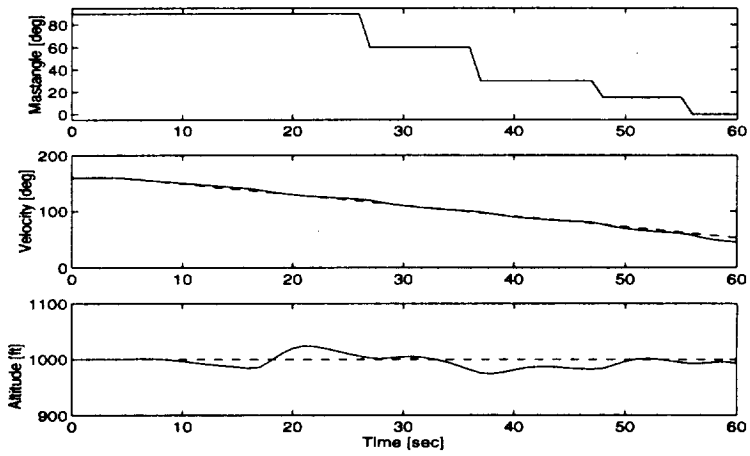

Figure 32: Conversion from forward flight into transition with a $-.1G$ *force* deceleration. Mast angle, velocity and altitude profiles.

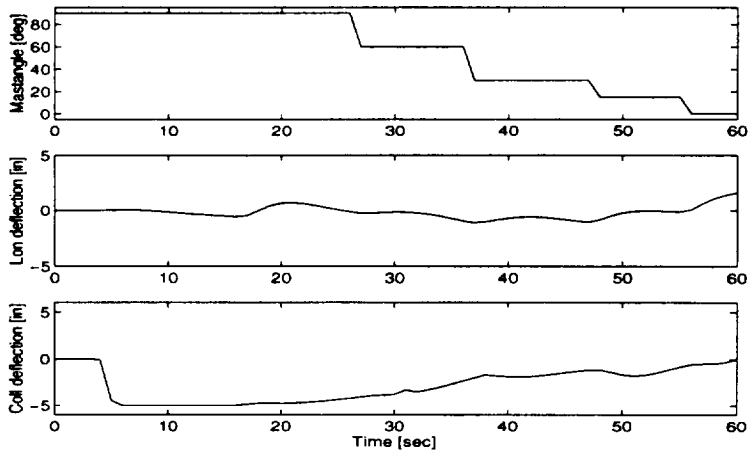

Figure 33: Conversion from forward flight into transition with a $-.1G$ *force* deceleration. Mast angle, and pilot activity.

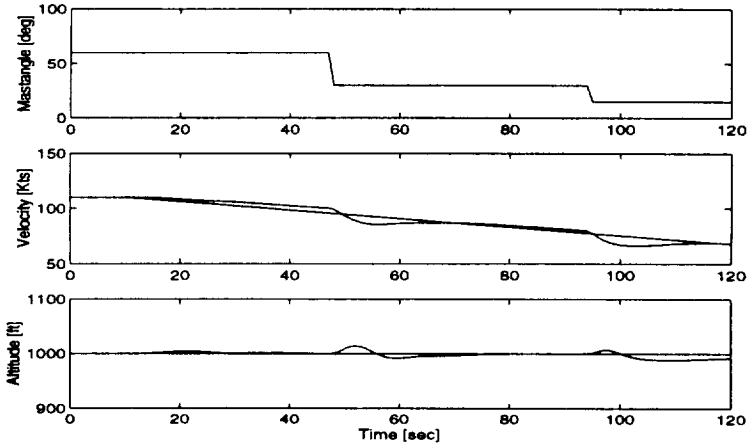

Figure 34: Conversion from transition flight into helicopter configuration. Mast angle, velocity and altitude profiles.

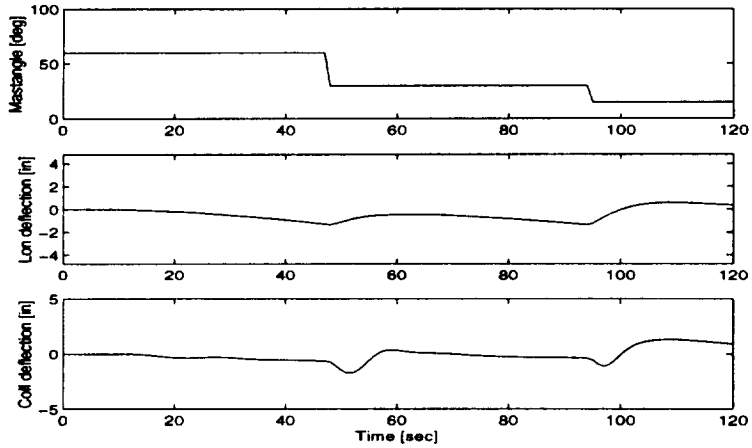

Figure 35: Conversion from transition flight into helicopter configuration. Mast angle, and pilot activity.

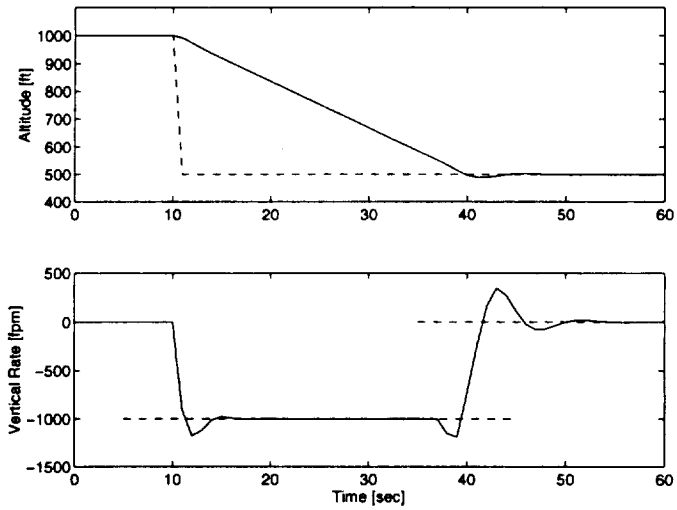

Figure 36: Simulated final approach descent at 30 Kts in helicopter configuration.

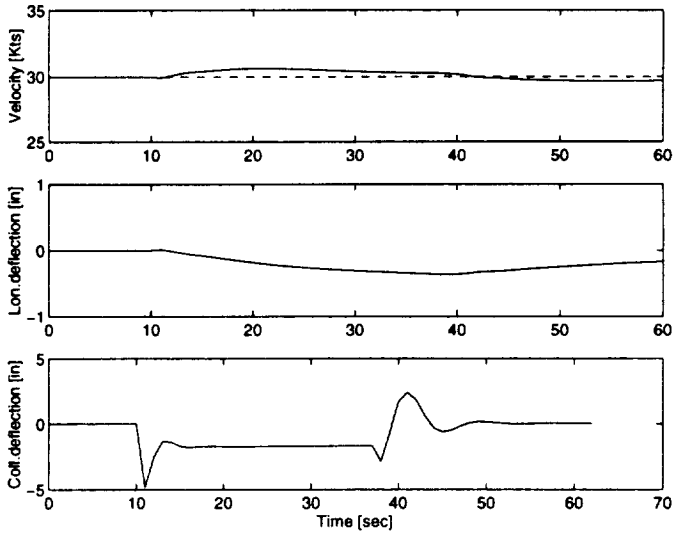

Figure 37: Velocity error and control activity during a final approach descent at 30 Kts in helicopter configuration.

3.4 Conclusion

A set of low order pilots models was developed for longitudinal operation of a tiltrotor aircraft. The combination of pilot models is capable of;

- operating on both sides of powercurve,
- following desired altitude profiles,
- following desired speed profiles,
- conversion both ways, achieved with reasonable tracking,
- fairly aggressive accelerations and climb rates.

Furthermore, the pilot can be adjusted for different operating circumstances. The requirement of operating on both sides of the power curve necessitates a shift in control strategies by the pilot. This change is reflected in the blending of the pilot models designed for the low speed helicopter configuration with those for the high speed airplane configuration. The results are adequate for smooth operation representative of non-aggressive pilot actions. More aggressive maneuvres are possible but will require some adjustements of the parameters. The coupling between altitude and speed control in airplane mode was reduced by using energy feedback for the throttle pilot model. The pole placement for the aircraft pilot models in this mode was more restrictive than in the helicopter configuration. Pitch rate feedback might improve upon this, but feedback of pitch rate

in the pilot model blurs the distiction between the pilot model and the operation of the SCAS system.

Because of symmetry of the XV15 there is no significant cross coupling between longitudinal and lateral modes. This allows for a seperate control architecture development and implementation in the longitudinal channels. A lateral set of pilot models needs to be developed to provide for coordinated turns and curved approach profiles.

4 Implementation of Neural Net Work Augmented Model Inversion

4.1 Neural Network Augmented Model Inversion

This section contains the highlights of the neural network augmented model inversion as applied to the tiltrotor aircraft. It is based on the applications as described in references [1] and [6]. It is included here to explain the concepts and indicate the results that are obtainable in the civil tiltrotor application. Figure 38 contains the architecture used for implementation of ACAH control in the pitch channel. Although model inversion is applied in all attitude channels, only the pitch channel was augmented with a neural network. In general, the pitch-roll-yaw axes for this aircraft are fairly well decoupled and similar performance of the adaptive system is expected in the roll and yaw axes when full implementation is considered at a later date. The simulation results presented here are based on a linear model for the XV-15 aircraft at different flight conditions, which includes the coupled six degrees-of-freedom dyamics together with the rotor dynamics. The model inversion is based on the linearized dynamics at 30 knots, with the rotor dynamics residualized. The primary purpose here is to demonstrate that the pitch channel neural network is capable of adapting to modeling errors in the linearized model. Unmodelled dynamics are represented by the fact that the rotor dynamics are residualized when deriving the nominal inverting controller.

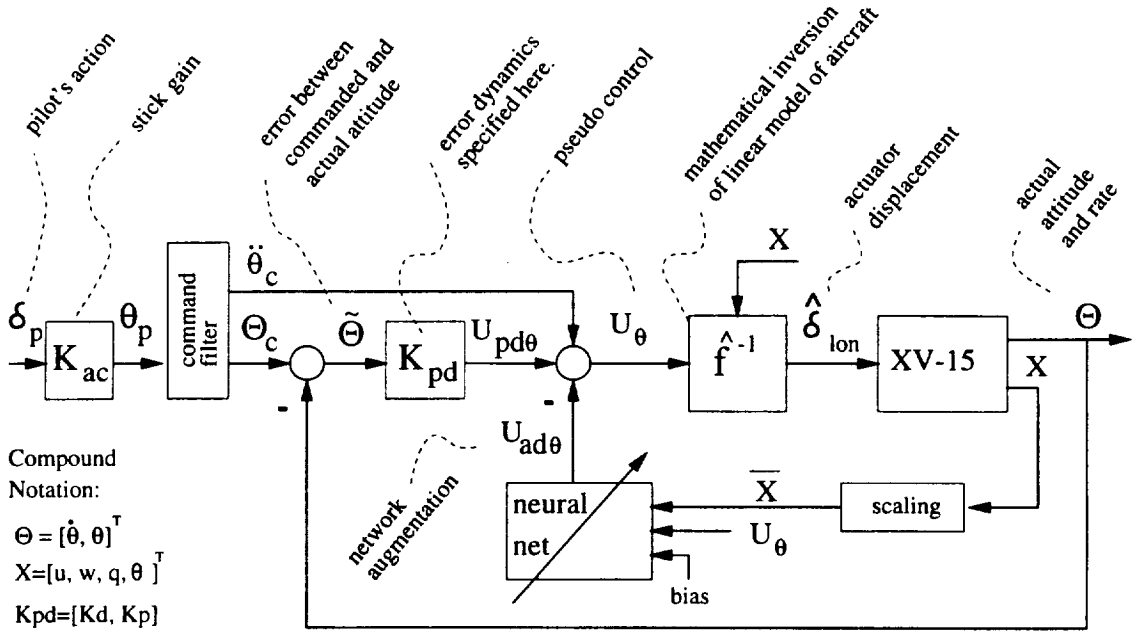

Figure 38: Neural network augmented model inversion architecture for the implementation of longitudinal ACAH control.

The neural network can consist of any linearly parameterized feedforward structure which is capable of approximately reconstructing the inversion error. For this demonstration a two layer sigma-pi network was used [1]. The inputs to the network consist of the longitudinal state variables, the pseudo control (U_θ) and a bias term.

The approximate inversion ($\hat{f}^{-1}$) is based on a linear model of the rotational dynamics of the XV-15.

$$\begin{Bmatrix} \dot{p} \\ \dot{q} \\ \dot{r} \end{Bmatrix} = A_1 \cdot \begin{Bmatrix} u \\ v \\ w \\ \delta_{col} \end{Bmatrix} + A_2 \cdot \begin{Bmatrix} p \\ q \\ r \end{Bmatrix} + B \cdot \begin{Bmatrix} \delta_{lat} \\ \delta_{lon} \\ \delta_{ped} \end{Bmatrix} \tag{18}$$

The states of interest for the augmentation are the Euler angular attitudes, and in particular the longitudinal attitude θ and its primary control δ_{lon}. In order to implement an ACAH system we consider inversion control using equation (18). This involves replacing the left hand side of the equation with commanded angular accelerations and solving for the control perturbations. From the control architecture in figure 38 the pseudo control for the three rotational degrees of freedom was designed in terms of Euler angles as:

$$U = \begin{Bmatrix} U_\phi \\ U_\theta \\ U_\psi \end{Bmatrix} = \begin{Bmatrix} U_{pd\phi} \\ U_{pd\theta} \\ U_{pd\psi} \end{Bmatrix} + \begin{Bmatrix} \ddot{\phi}_c \\ \ddot{\theta}_c \\ \ddot{\psi}_c \end{Bmatrix} - \begin{Bmatrix} 0 \\ U_{ad\theta} \\ 0 \end{Bmatrix} \tag{19}$$

Here $U_{ad\theta}$ is an adaptive signal which represents the neural network augmentation in the pitch channel, and the proportional-derivative control for the longitudinal channel is designed as:

$$U_{pd\theta} = K_d \cdot (\dot{\theta}_c - \dot{\theta}) + K_p \cdot (\theta_c - \theta) \tag{20}$$

The gains K_p and K_d are used to define the error dynamics. The quantities θ_c and $\dot{\theta}_c$ are outputs of the command filter, whose parameters are chosen based on handling quality criteria. Thus the command filter serves both to limit the input rate, and as a model for desired response.

To use the pseudo control in equation (18) it needs to be transformed from the Euler frame to the body axes. In terms of the individual components, the equivalent body angular acceleration commands are computed as:

$$\begin{aligned} \dot{p}_c &= U_\phi - U_\psi s_\theta - \dot{\psi}\dot{\theta}c_\theta \\ \dot{q}_c &= U_\theta c_\phi - \dot{\theta}\dot{\phi}s_\phi + U_\psi s_\phi c_\theta + \dot{\psi}\dot{\phi}c_\phi c_\theta - \dot{\psi}\dot{\theta}s_\phi s_\theta \\ \dot{r}_c &= -U_\theta s_\phi - \dot{\theta}\dot{\phi}c_\phi + U_\psi c_\phi c_\theta - \dot{\psi}\dot{\phi}s_\phi c_\theta - \dot{\psi}\dot{\theta}c_\phi s_\theta \end{aligned} \tag{21}$$

where s_ϕ is shorthand for $sin\phi$, etc. Replacing the left hand side of equation (18) with $\{\dot{p}_c, \dot{q}_c, \dot{r}_c\}^T$ and inverting gives:

$$\begin{Bmatrix} \delta_{lat} \\ \delta_{lon} \\ \delta_{ped} \end{Bmatrix} = B^{-1} \cdot \{ \begin{Bmatrix} \dot{p}_c \\ \dot{q}_c \\ \dot{r}_c \end{Bmatrix} - A_1 \cdot \begin{Bmatrix} u \\ v \\ w \\ \delta_{col} \end{Bmatrix} - A_2 \cdot \begin{Bmatrix} p \\ q \\ r \end{Bmatrix} \} \tag{22}$$

Because in practice $A1$, $A2$, and B are not represented exactly we actually obtain $\hat{\delta}$.

$$\begin{Bmatrix} \hat{\delta}_{lat} \\ \hat{\delta}_{lon} \\ \hat{\delta}_{ped} \end{Bmatrix} = \hat{B}^{-1} \cdot \{ \begin{Bmatrix} \dot{p}_c \\ \dot{q}_c \\ \dot{r}_c \end{Bmatrix} - \hat{A}_1 \cdot \begin{Bmatrix} u \\ v \\ w \\ \delta_{col} \end{Bmatrix} - \hat{A}_2 \cdot \begin{Bmatrix} p \\ q \\ r \end{Bmatrix} \} \tag{23}$$

The inversion error in this case is defined as:

$$\epsilon = \begin{Bmatrix} \dot{p} \\ \dot{q} \\ \dot{r} \end{Bmatrix} + -\hat{A}_1 \cdot \begin{Bmatrix} u \\ v \\ w \\ \delta_{col} \end{Bmatrix} - \hat{A}_2 \cdot \begin{Bmatrix} p \\ q \\ r \end{Bmatrix} - \hat{B} \cdot \begin{Bmatrix} \hat{\delta}_{lat} \\ \hat{\delta}_{lon} \\ \hat{\delta}_{ped} \end{Bmatrix} \tag{24}$$

We may equivalently represent the effect of ϵ in the pitch attitude dynamics as:

$$\ddot{\theta} = U_\theta + \epsilon_\theta \tag{25}$$

Combining equations (19), (20) and (25) we have:

$$\ddot{\tilde{\theta}} + K_d \cdot \dot{\tilde{\theta}} + K_p \cdot \tilde{\theta} = U_{ad\theta} - \epsilon_\theta \tag{26}$$

where $\tilde{\theta} = \theta_c - \theta$, and ϵ_θ is the pitch component of the inversion error when represented in the Euler frame. In the ideal case, the neural network output cancels ϵ_θ.

Neural Network Architecture

The input/output map of the neural network may be represented as,

$$U_{ad\theta} = W^T \beta(\bar{X}, U_\theta) \tag{27}$$

where W is a vector of network weights, and β is a vector of network basis functions. The basis functions are chosen from a sufficiently rich set of functions so that the inversion error function, ϵ_θ, can be accurately reconstructed at the network output. The basis functions were constructed by grouping the inputs into three categories. The first category consists of,

$$C_1 = \{1,\ V,\ V^2\} \tag{28}$$

where V is the airspeed. This is used to model inversion error due to changes in airspeed. In the linearized simulation, the stability and control derivative are airspeed dependent. The second category consists of state variables and the pseudo control.

$$C_2 = \{1,\ u,\ w,\ q,\ \theta, U_\theta\} \tag{29}$$

The third category is used to approximate higher order effects due to changes in pitch attitude. This is largely due to the transformation between the body frame and the inertial frame.

$$C_3 = \{1,\ \theta\} \tag{30}$$

The vector of basis functions is composed of all possible products of the elements of C_1, C_2, and C_3,

$$\beta = kron(kron(C_1, C_2), C_3) \tag{31}$$

where,

$$kron(x, y) = [x_1 y_1 \; x_1 y_2 \; .....x_m y_n]^T \tag{32}$$

The network weights are adapted on-line according to the following equation,

$$\dot{W} = -\gamma s \beta \tag{33}$$

where $\gamma > 0$ is the adaptation gain and,

$$s = \frac{1}{2K_p}\tilde{\theta} + \frac{1}{2 \cdot \lambda \cdot K_p}\dot{\tilde{\theta}} \tag{34}$$

$$\lambda = \frac{K_d}{1 + K_p} \tag{35}$$

The adaptation law was originally designed based on a Lyapunov stability analysis of the error signals [6], which relies on the use of a deadzone in which the adapation law is turned off when a weighted norm of the error signals is small. The purpose of the deadzone is to account for the fact that the network can not exactly reconstruct the functional form of inversion error. However, we did not implement the deadzone in this study. This gives an indication that the basis functions chosen above are sufficiently rich when an instability is not observed. In practice, the deadzone should be employed to as a safeguard against the occurance of an instability.

4.2 Numerical Results

The model inversion control, as given by equation (23), was applied to the XV-15 with the aerodynamics, linearized about the 30 Kts level flight helicopter configuration. The XV-15 model itself is for this proof of concept approximated by the GTRS code also linearized about 30 Kts. The latter linearization includes rotor states. These states are subsequently residualized, to determine the approximate values of $A1$, $A2$ and B, at 30 Kts. The model inversion therefore assumes the rotor is in a quasi steady state. A third order command filter was used, so that $\ddot{\theta}_c$ is continuous for a step in θ_p, see figure 38. The dominant complex poles of the filter provide minimal overshoot ($\zeta = .8$) and a 5% settling time of 1.5 seconds ($\omega_n = 2.5 rad/sec$), which provide level 1 handling characteristics in the pitch channel [7]. The gains K_p and K_d were chosen so that the error dynamics settle in 1 second ($\zeta = .8$, $\omega_n = 3.75 rad/sec$). The cases with NNW augmentation are with an adaptation gain of $\gamma = 1000$.

Model Inversion at 30 Kts

The results in figures 39 through 42 represent model inversion at 30 Kts, without NNW augmentation (dashed lines) and with the NNW (dash-dot lines). The pitch response with NNW augmentation is barely distinguishable from the commanded pitch input (solid line) in figure 39. The corresponding actuator activity is given by figure 40. The figure shows the total range of

the full authority actuator, approximately -4.8 *inches* to $+4.8$ *inches*. Figures 41, and 42 show respectively the pitch augmentation error, $U_{ad\theta}(t) - \epsilon_\theta(t)$ and the NNW weights associated with the linear terms from the category two list in equation (29). Note that the inversion error (ϵ_θ) is effectively cancelled by the NNW output in figure 41.

NNW Compensation for Modeling Uncertainties

The ability of the adaptive control architecture to compensate for inversion error is indicated in figures 43 through 54. Figures 43 through 46 show the responses for operation at 30 Kts with a simulated inversion error. The inversion error was implemented by scaling the aerodynamic stability derivative M_q to 150% and the control derivative $M_{\delta lon}$ to 50% of their exact values. The model inversion control is thus based on reduced control effectiveness and increased pitch damping. These effects are visible by comparing the results of the nominal case in figures 39 through 42 to these results.

The ability of the adaptive control architecture to compensate for inversion error due to operation at a different operating point while using model inversion based at 30 Kts is indicated in figures 47, through 54. Two cases are shown. The first case is configured at hover, and the second at 100 Kts with a mast angle converted 60 degrees from helicopter configuration, and the flap/flaperons set to 20/12.5 degrees. The effects of using model inversion without the NNW compensation (dashed lines) are small, indicating that inversion error due to changes in operating point are small. The responses with the NNW in figures 47 and 51 are again barely distinguishable from the command, indicating that the NNW is functioning properly. In particular, the pitch augmentation error is reduced to zero in both cases. These results indicate how the control architecture applied here can alleviate the need for gain scheduling. What is not directly apparent from these linear model based demonstrations are the effects of trim changes, e.g. in going from 30 Kts to 100 Kts, through conversion. This will be evaluated using GTRS in the next phase of the effort.

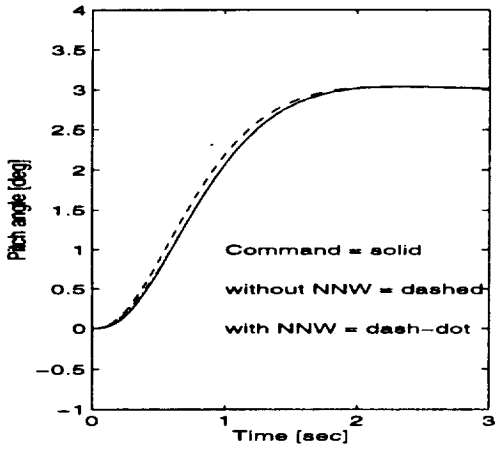

Figure 39: Pitch angle response at 30 Kts.

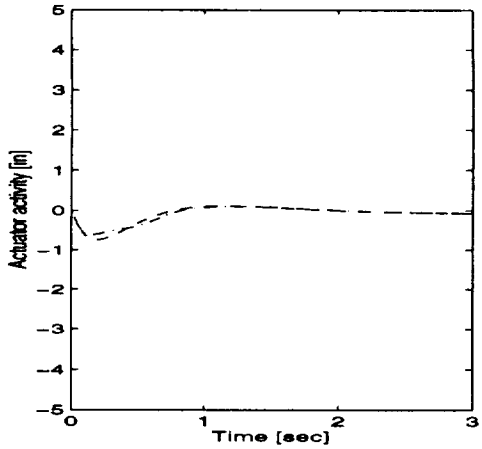

Figure 40: Actuator activity at 30 Kts.

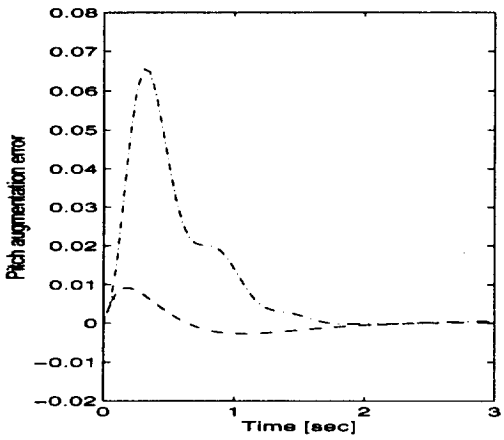

Figure 41: Pitch augmentation error at 30 Kts.

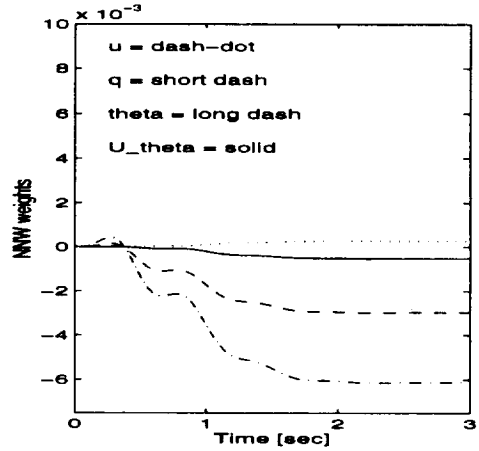

Figure 42: NNW weight adaptation time histories.

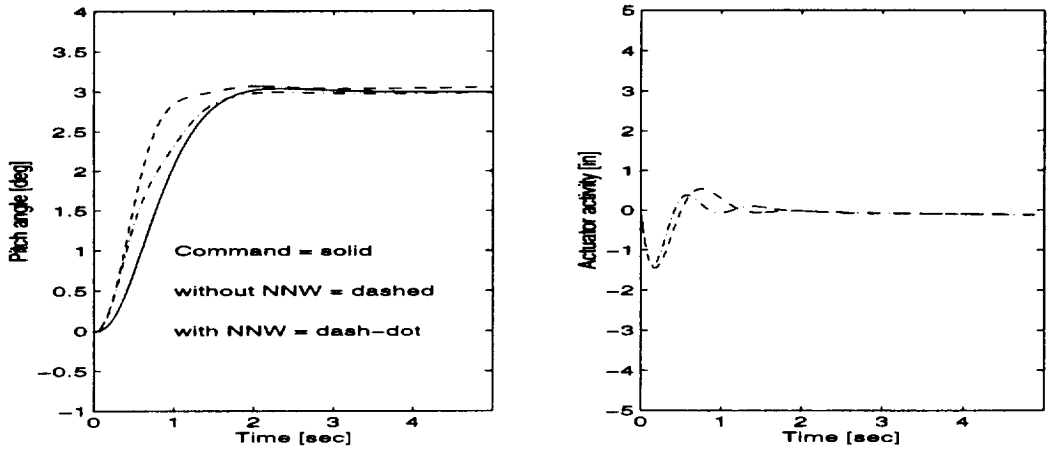

Figure 43: Pitch angle response at 30 Kts with errors in inversion model.

Figure 44: Actuator activity at 30 Kts with errors in inversion model.

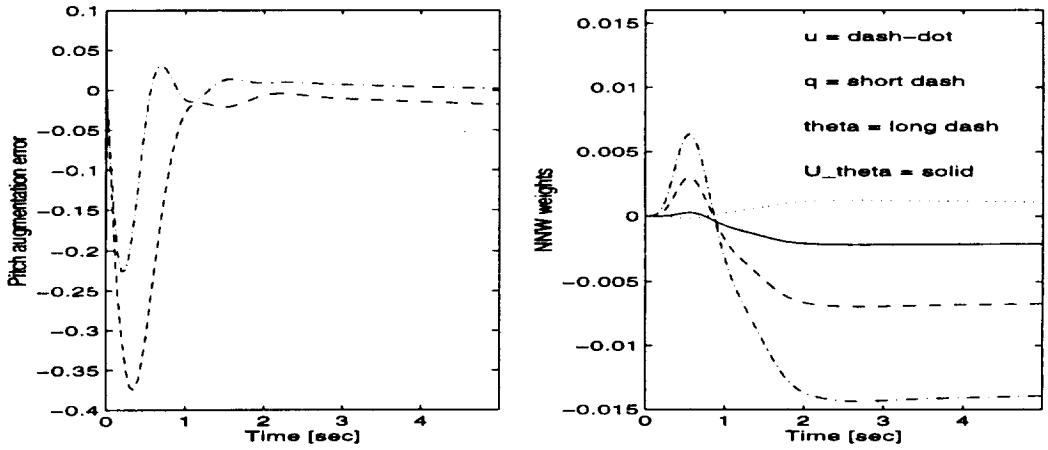

Figure 45: Pitch augmentation error at 30 Kts with errors in inversion model.

Figure 46: NNW weight adaptation time histories.

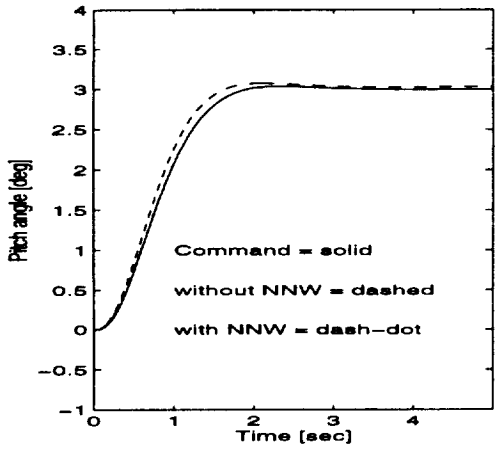

Figure 47: Pitch angle response at hover with model inversion based on 30 Kts.

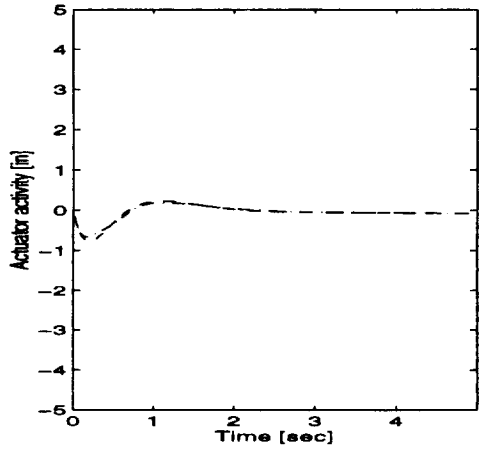

Figure 48: Actuator activity at hover with model inversion based on 30 Kts.

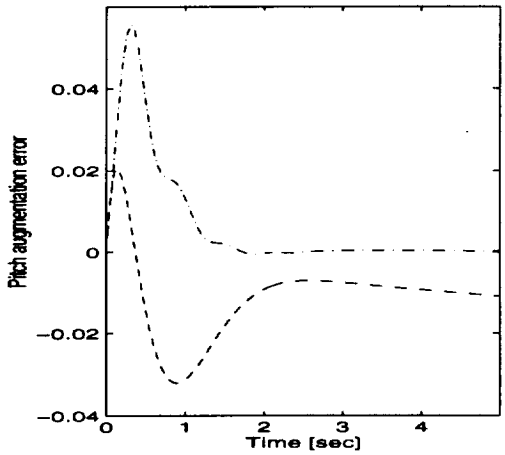

Figure 49: Pitch augmentation error at hover using model inversion based on 30 Kts.

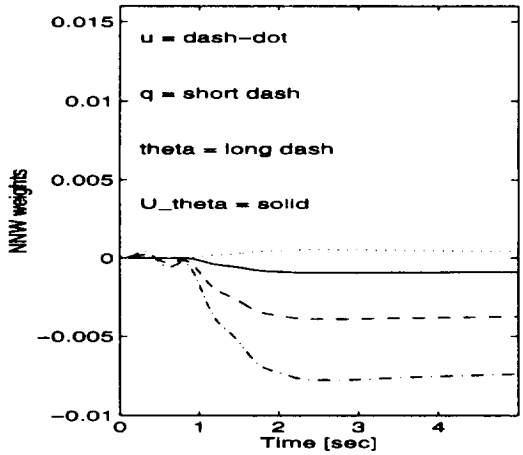

Figure 50: NNW weight adaptation time histories.

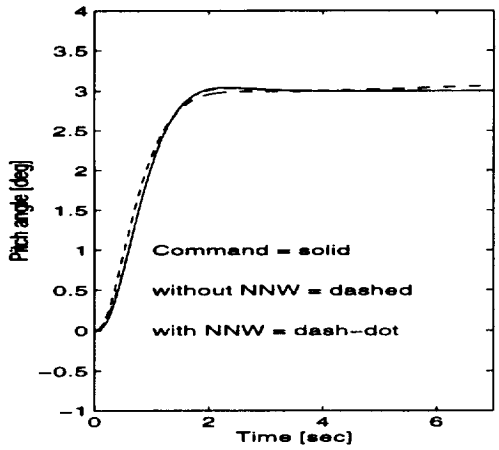

Figure 51: Pitch angle response at 100 Kts with model inversion based on 30 Kts.

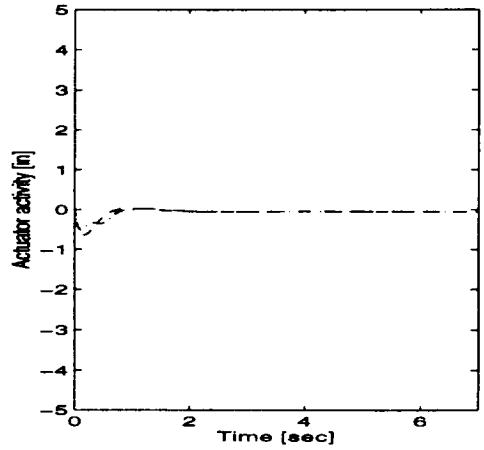

Figure 52: Actuator activity at 100 Kts with model inversion based on 30 Kts.

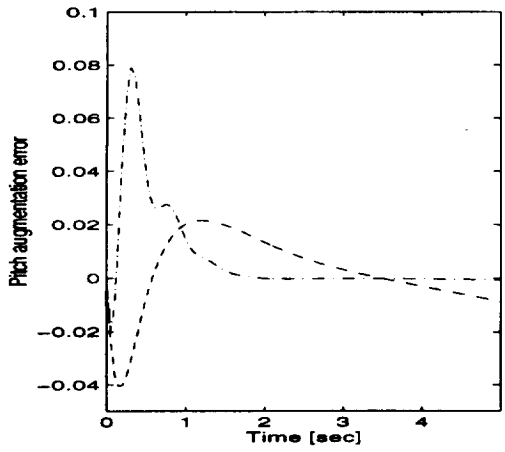

Figure 53: Pitch compensation error at 100 Kts with model inversion based on 30 Kts.

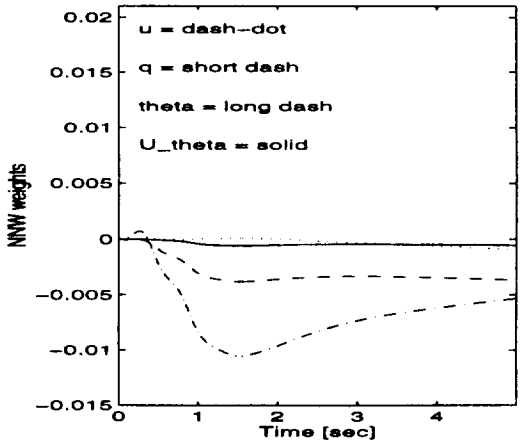

Figure 54: NNW weight adaptation time histories.

5 Further Development

The second year of the research effort will concentrate on a logical extension of the developments to date. The set of pilot models shall be extended to the lateral channels to provide heading hold at the lower speeds and coordinated turns at the higher velocities. The development of the NNW-based controllers will first be evaluated in linear simulation, followed by implementation and evaluation in the PC Fortran environment of the GTRS code. The linear simulation will allow for a thorough evaluation of the various aspects of the architecture as described in section 4.1. What will not be directly apparent from these linear model based demonstrations is the effects of trim changes. These trim changes are relatively slow and the NNW is capable of compensating for these changes. In fact, this will likely be one of the biggest contributions of the NNW, alleviating the need for extensive scheduling with different flight configurations. It is expected that NASA AMES will provide support in the form of recommendations as to the approach procedures and required handling characteristics applicable to a civil tiltrotor. Furthermore, recommendations relative to our initial development of a pilot model can be implemented at early stage.

In particular, the year-2 effort will include the following tasks:

Task 1: Completion of the pilot modeling task. This includes the development of a pilot model set for the lateral channels to provide for coordinated turns or heading hold. This will provide for a total set of low order pilot models able to perform 3 dimensional approach profiles at varying levels of descent rates.

Task 2: Development of the NNW-based control architecture for a Rate-Command Attitude-Hold as compared to the Attitude-Command Attitude-Hold presently developed for the pitch channel. This includes both longitudinal and lateral channels. The initial development will be done using a set of linearized models, followed by implementation in the GTRS simulation code.

Task 3: Development of separate fully automated NNW-based controller channels, leading to fully automated approach capability. This development will be done using only the GTRS simulation code.

Task 4: Development of performance measures and subsequent evaluation, including the effects of partial failures.

Possible deficiencies inherent to the present approach that may be due to practical implementation issues, or to issues particular to civil tiltrotor applications, will be identified. It is hoped that the cooperative effort will in this manner provide an important step in bridging the gap between theory and application of neural network based flight control system design.

References

[1] Byoung Soo Kim. *Nonlinear Flight Control Using Neural Networks.* Phd thesis, Georgia Institute of Technology, School of Aerospace Engineering, Atlanta, Georgia, December 1993.

[2] Jesse Leitner. *Helicopter Nonlinear Control Using Adaptive Feedback Linearization.* Phd thesis, Georgia Institute of Technology, School of Aerospace Engineering, May 1995.

[3] Kevin W. Goldstein and L.W. Dooley. V-22 Control Law Development. In *AHS 42nd Annual Forum, Washington, D.C.*, June 1986.

[4] MIL-F-83300. *Military Specifications for Flying Qualities of Piloted V/STOL Aircraft*, March 1971.

[5] William A. Decker. Piloted Simulator Investigations of a Civil Tilt-Rotor Aircraft on Steep Instrument Approaches. In *AHS 48th Annual Forum, Washington, D.C.*, June 1992. NASA Ames Research Center, Moffett Field, California.

[6] Byoung Soo Kim and A.J. Calise. Nonlinear Flight Control Using Neural Networks. *AIAA Journal of Guidance, Navigation and Control*, 20(1), Jan/Feb 1997. To be published.

[7] Gary B. Churchill and R.M. Gerdes. Advanced AFCS Developments on the XV-15 Tilt Rotor Research Aircraft. In *AHS 40th Annual Forum, Arlington, VA*, May 1984.